

Transformer Current Ringing in Dual Active Bridge Converters

Qin, Z.; Shen, Zhan; Blaabjerg, Frede; Bauer, P.

DOI

[10.1109/TIE.2020.3040681](https://doi.org/10.1109/TIE.2020.3040681)

Publication date

2020

Document Version

Accepted author manuscript

Published in

IEEE Transactions on Industrial Electronics

Citation (APA)

Qin, Z., Shen, Z., Blaabjerg, F., & Bauer, P. (2020). Transformer Current Ringing in Dual Active Bridge Converters. *IEEE Transactions on Industrial Electronics*, 68(12), 12130-12140. Article 9280428. <https://doi.org/10.1109/TIE.2020.3040681>

Important note

To cite this publication, please use the final published version (if applicable).
Please check the document version above.

Copyright

Other than for strictly personal use, it is not permitted to download, forward or distribute the text or part of it, without the consent of the author(s) and/or copyright holder(s), unless the work is under an open content license such as Creative Commons.

Takedown policy

Please contact us and provide details if you believe this document breaches copyrights.
We will remove access to the work immediately and investigate your claim.

Transformer Current Ringing in Dual Active Bridge Converters

Zian Qin, *Senior Member, IEEE*, Zhan Shen, *Member, IEEE*, Frede Blaabjerg, *Fellow, IEEE*, Pavol Bauer, *Senior Member, IEEE*

Abstract— In Dual Active Bridge (DAB) converters, there can be transformer current ringing, especially when the transformer turns ratio is high. It is induced by high dv/dt generated by fast switching as well as the low impedance of the magnetic tank at the high-frequency range. To quantify the influence of the magnetic tank, its impedance model is thoroughly modeled by considering all the parasitic components. It is found that the parasitic capacitors of the magnetics do not equally affect the current ringing, and thereby the critical one is addressed. On top of that, the design guide of the inductor is provided for mitigation of the current ringing. Additionally, the impact of dv/dt is also studied. The models and analyses are verified on a 2.5 kW DAB prototype.

Index Terms — dual active bridge converter, current ringing, impedance model, magnetic tank, dv/dt

I. INTRODUCTION

THE DAB converter [1], due to its simple topology and control, galvanic isolation, bidirectional power flow, wide input and output voltage adaptive range, high power density, and efficiency, is very promising in applications like Solid State Transformers (SST) [2-4], electric vehicle chargers with V2G concept [5][6], power flow control in DC grids [7-9], etc.

DAB is known as a converter with soft-switching, but when the load is very light, or the input/output voltage deviates a lot from the rated value, it can hardly maintain soft-switching. Then not only the power loss is increased, but also EMI issues get worse. Various modulation strategies were, therefore, proposed to extend the soft-switching region [10][11][12].

Wide bandgap device based DAB were studied in literature not only for higher efficiency, but mainly for either higher voltage rating like SiC-based DAB in SSTs [2], or more compact design like GaN-based DAB in an on-board charger [5]. In both scenarios, dv/dt is pushed to very high. Then EMI issues become more critical [13][14]. The reason is that the magnetic tank of the DAB, as shown in Fig. 1, has parasitic capacitance, which changes the impedance of the magnetic tank from inductive to capacitive at high frequency, where the impedance has a shallow magnitude. Together with a high dv/dt , the current ringing and thereby EMI become significant. The current ringing may also lead to more power loss in the converter since the ac resistance of the wire at the ringing frequency is much higher than the fundamental frequency [15].

The current ringing issues can be eliminated by adding parallel capacitance to the switches to reduce dv/dt [13], where

the full parasitic model of the transformer is also considered in the impedance modeling. However, the turn-on switching loss will increase when the converter enters into hard-switching, and a larger capacitor in parallel also makes the soft-switching more challenging to achieve since more energy is needed to discharge the capacitor. Moreover, lower dv/dt limits the switching frequency in terms of duty ratio loss. Finally, in practice, one or two series inductors are needed in the magnetic tank for the power flow control, which contributes considerable stray capacitance and should also be considered [15].

Another promising method to decrease the current ringing is to improve the impedance of the magnetic tank. Therefore, detailed modeling of the parasitics of the magnetic tank, i.e., stray capacitance, leakage inductance, and ac resistance, is essential. For the stray capacitance modeling, various structure-based analytical methods are reviewed in [16]. The impact of the various winding architectures and wire types is discussed in [17-24]. The stray capacitance of planar transformers is a severe issue, and the tradeoff between the stray capacitance, ac resistance, and leakage inductance is discussed in [25][26][27]. For the ac resistance of winding, Dowell has proposed the classic formula, which considers both the skin and proximity effect in the high-frequency range [28]. It assumes that the magnetic flux is straight, and is modified and improved by considering the flux distortion [29][30] and the phase shift of the current [31] in recent advances. The analytical model of the Litz wire winding resistance is proposed in [32]. The analytical leakage inductance models are also based on the physical structure of magnetics. Dowell also gives the one-dimensional expression of leakage inductance in [28]. It is later developed by considering the more detailed winding and core structure into the analysis [35]. Further, the leakage inductance of magnetics with Litz wire [38], unparallel winding [39], non-idea winding [24], and different winding shape and configurations [40][41][42] are investigated through the detailed magnetic field flux modeling, respectively. In general, those researches focus on the physical-structure-based parasitic modeling of single magnetic components. Their models can be used in the inductor-transformer combined magnetic tank modeling in this study at the circuit level.

At the circuit level, [26][43][44] have verified that by decreasing the stray capacitance of magnetics, the current ringing, as well as the measured EMI reduces dramatically. Research in [45] solves this issue by improving the layout of the planar transformer. The concept of the paired layer is proposed in [46], and it achieves small dv/dt as well as a significant reduction of common-mode (CM) noise in the flyback and forward converter. The transformer capacitance network of a flyback converter is also studied in [47] to reduce

Zian Qin and Pavol Bauer are with the Department of Electrical Sustainable Energy, DCE&S group, Delft University of Technology, Mekelweg 4, 2628 CD, Delft, the Netherlands. (email: Z.Qin-2@tudelft.nl, P.Bauer@tudelft.nl)

Zhan Shen and Frede Blaabjerg are with the Department of Energy Technology, Aalborg University, 9220 Aalborg, Denmark (email: zhs@et.aau.dk, fbl@et.aau.dk). (Corresponding author: Zhan Shen.)

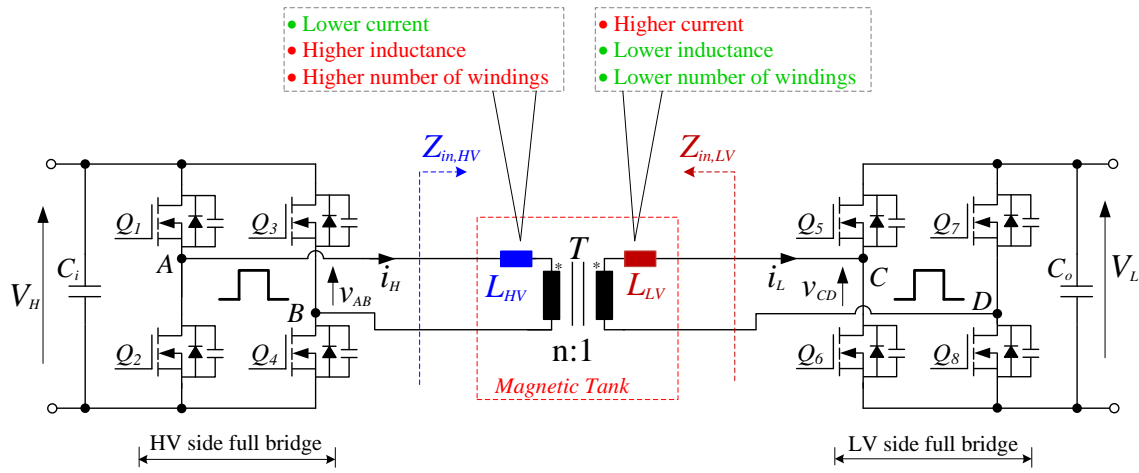


Fig. 1. A dual active bridge converter (DAB). To realize the large leakage inductance of the transformer T for power transforming, a stand-alone inductor is added to the high voltage side (L_{HV}), low voltage side (L_{LV}), or both sides.

its CM noise. Further, the Faraday shield is a powerful structure to minimize the transformer inter-winding capacitance as well as the CM noise [47][48]. Moreover, by precisely controlling the leakage inductance in the DAB [49] and LLC resonant converter [50], the circuit performance, control flexibility, and efficiency are improved. However, for those methods, a specific analysis and design of the transformer layer structure are needed. For the active solution of the current ringing mitigation, research in [51] uses the active harmonic suppression strategy in the modulation to decrease the DC bus harmonic of DAB.

Yet in those studies, only the impact of the sole parasitic of the single magnetic component is considered. A quantified model in the inductor-transformer combined magnetic tank considering all parasitics, i.e., the stray capacitance, leakage inductance, and ac resistance, and their impacts on various high-frequency aspects, e.g., current ringing, EMI, efficiency, is still rare.

Our previous conference work presents a simple model of the magnetic tank [52]. In this paper, a more complete and concrete impedance modeling and analysis are presented, where the impact of the different parasitic capacitors in the magnetic tank is quantified to address the critical one. Moreover, the leakage inductance and the equivalent resistance are also considered. Further, the impact of dv/dt on the current ringing is also quantified, and the experimental verification is enriched. The results can be used as a guide for the converter designer. The rest of the paper is organized as follows: the impedance of the magnetic tank is modeled in Section II; then based upon the model the current ringing is analyzed in Section III, where the mitigation measure is also discussed and design guide is provided; the work is then verified in Section IV, and concluded in Section V.

II. MAGNETIC TANK IMPEDANCE MODELING

As shown in Fig. 1, a DAB converter is composed of two full bridges and a magnetic tank. The former contains eight power switches $Q_1 \sim Q_8$ and two capacitors C_i and C_o . v_{AB} and v_{CD} are the two voltages generated by the HV and LV side full bridge, respectively. The magnetic tank includes a transformer T and an inductor. The stand-alone inductor is to add the

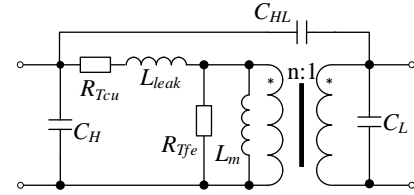
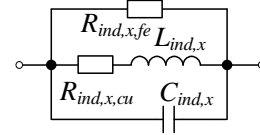


Fig. 2. The impedance model of a two-winding transformer.



Note: x can be H or L

Fig. 3. The impedance model of an inductor.

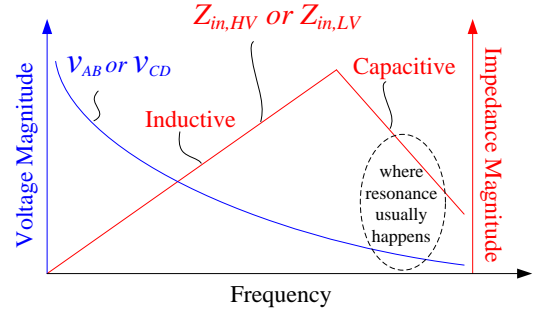


Fig. 4. A diagram to show the spectrum of the input voltage and impedance of the magnetic tank.

leakage inductance of the transformer with smaller power loss compared to a single transformer with considerable leakage. In literature, the inductor has been connected to the high voltage winding, low voltage winding, or both. There are pros and cons to connect the inductor differently, as summarized in Fig. 1. But how they can influence the transformer current ringing is unclear. Thus, to make the analysis more generic, it is assumed that the inductor is split into two, L_{HV} and L_{LV} for high and low voltage windings, respectively, and their equivalent inductances are identical. $Z_{in,HV}$ and $Z_{in,LV}$ are the input

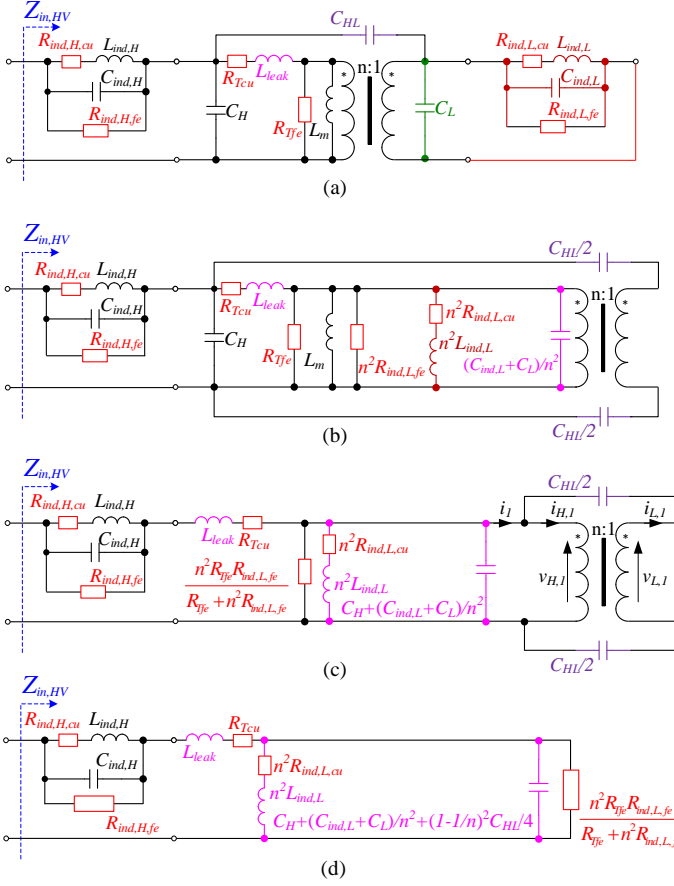


Fig. 5. HV side input impedance model of the magnetic tank (a) detailed model (b) intermediate model 1 (c) intermediate model 2 (d) simplified model.

impedance of the magnetic tank at high and low voltage side, respectively. Then the current ringing on the HV side is influenced by the dv/dt on HV side and $Z_{in,HV}$, while the current ringing on LV side is influenced by the dv/dt on LV side and $Z_{in,LV}$.

The generic impedance models of transformer and inductor are used for analysis, and they are shown in Fig. 2 and Fig. 3. In the transformer model, L_m is the magnetizing inductance; L_{leak} is the leakage inductance; C_H and C_L are the HV and LV side winding capacitance; C_{HL} is the coupling capacitance between the two windings; R_{Tcu} is the winding resistance; R_{Tfe} is the equivalent resistance indicating the core loss. The inductor model is composed of an inductor $L_{ind,x}$, a capacitor $C_{ind,x}$ in parallel, a winding resistance $R_{ind,x,cu}$, and an equivalent resistance $R_{ind,x,fe}$ regarding the core loss. At low frequency, the inductance dominates the impedance, while at high frequency, the capacitance will take over. So both $Z_{in,HV}$

$$Z_{in,HV}|_{L_{ind,L}=0} = \frac{R_{ind,H,fe}(sL_{ind,H} + R_{ind,H,cu})}{s^2 L_{ind,H} C_{ind,H} R_{ind,H,fe} + s(L_{ind,H} + C_{ind,H} R_{ind,H,fe} R_{ind,H,cu}) + R_{ind,H,fe} + R_{ind,H,cu}} + sL_{leak} + R_{Tcu} \quad (1)$$

$$Z_{in,HV}|_{L_{ind,H}=0} = \frac{R_A(s^2 L_{ind,L} + n^2 R_{ind,L,cu})}{s^2 n^2 L_{ind,L} C_{ind,L} R_{ind,L,fe} + s^2 (L_{ind,H} + C_A R_A R_{ind,H,cu}) + R_A + n^2 R_{ind,H,cu}} + sL_{leak} + R_{Tcu} \quad (2)$$

$$Z_{in,LV}|_{L_{ind,L}=0} = \frac{R_B(sL_{ind,H} + R_{ind,H,cu})}{s^2 L_{ind,H} C_{ind,H} R_{ind,H,fe} + s(L_{ind,H} + C_B R_B R_{ind,H,cu}) + n^2 R_B + R_{ind,H,cu}} + \frac{sL_{leak}}{n^2} + \frac{R_{Tcu}}{n^2} \quad (3)$$

$$Z_{in,LV}|_{L_{ind,H}=0} = \frac{R_{ind,L,fe}(sL_{ind,L} + R_{ind,L,cu})}{s^2 L_{ind,L} C_{ind,L} R_{ind,L,fe} + s(L_{ind,L} + C_{ind,L} R_{ind,L,fe} R_{ind,L,cu}) + R_{ind,L,fe} + R_{ind,L,cu}} + \frac{sL_{leak}}{n^2} + \frac{R_{Tcu}}{n^2} \quad (4)$$

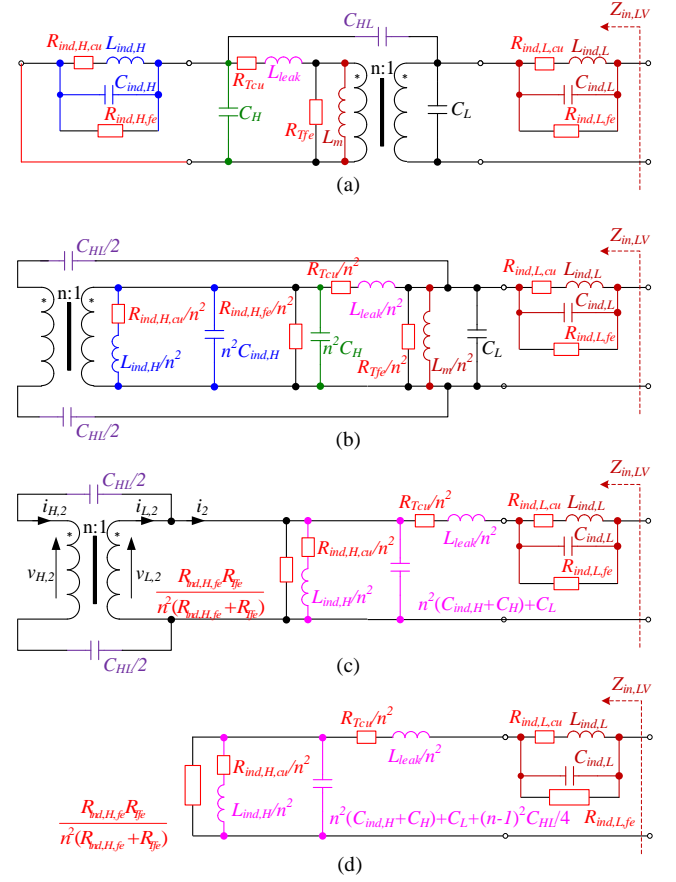
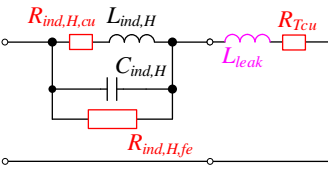
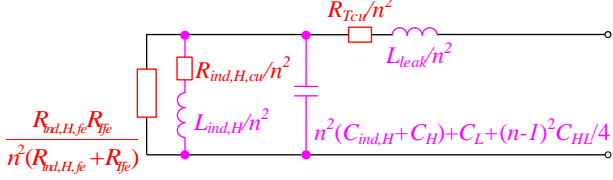
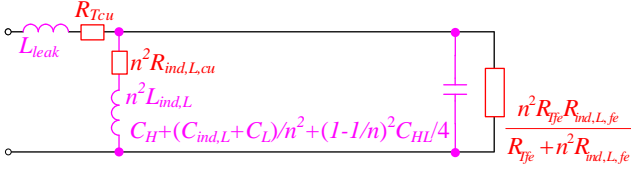
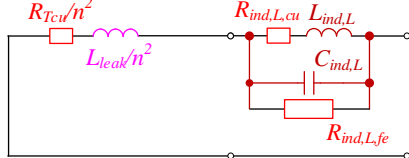


Fig. 6. LV side input impedance model of the magnetic tank (a) detailed model (b) intermediate model 1 (c) intermediate model 2 (d) simplified model.

and $Z_{in,LV}$ will have an impedance curve as depicted in Fig. 4. Depending on the modulation scheme (single phase shift, dual phase shift, triple phase shift) used in the DAB, the input voltage of the magnetic tank v_{AB} and v_{CD} can be both square, one square and one three-level hybrid, or both three-level waveforms. Regardless, v_{AB} and v_{CD} will have a spectrum as shown in Fig. 4. It can be seen that as frequency increases the magnitude of voltage harmonics will decrease and the impedance will increase, which makes the current ringing hardly happen below the corner frequency. But beyond that frequency, the impedance starts to decline, and it largely boosts the chance of current ringing. To concretely analyze the current ringing, the two impedances of the magnetic tank are thoroughly modeled, as shown in Fig. 5 and Fig. 6. The modeling procedure is elaborated in the Appendix.

Assuming the inductor is only connected to either the HV or LV side, then from Fig. 5(d) and Fig. 6(d), it can be obtained,

TABLE I. Impedance model of the magnetic tank.

Condition	Impedance	Comment
$Z_{in,HV} _{L_{ind,L}=0}$ Only HV side inductor		Only $C_{ind,H}$ matters. Design challenge is low
$Z_{in,LV} _{L_{ind,L}=0}$		The impact of C_H , $C_{ind,H}$ and C_{HL} are much amplified Design challenge is high
$Z_{in,HV} _{L_{ind,H}=0}$ Only LV side inductor		Mainly the C_H and C_{HL} influence. Design challenge is medium
$Z_{in,LV} _{L_{ind,H}=0}$		Only $C_{ind,L}$ matters Design challenge is low

$$R_A = \frac{n^2 R_{Tfe} R_{ind,L,fe}}{R_{Tfe} + n^2 R_{ind,L,fe}} \quad (5)$$

$$C_A = C_H + \frac{C_{ind,L} + C_L}{n^2} + (1 - 1/n)^2 C_{HL}/4 \quad (6)$$

$$R_B = \frac{R_{Tfe} R_{ind,H,fe}}{n^2 (R_{Tfe} + R_{ind,H,fe})} \quad (7)$$

$$C_B = n^2 (C_{ind,L} + C_H) + C_L + (n - 1)^2 C_{HL}/4 \quad (8)$$

where $Z_{in,HV}|_{L_{ind,L}=0}$ and $Z_{in,LV}|_{L_{ind,L}=0}$ depict the input impedance of the magnetic tank from HV and LV side, respectively, and meanwhile, the inductor is connected only on high voltage side; $Z_{in,HV}|_{L_{ind,H}=0}$ and $Z_{in,LV}|_{L_{ind,H}=0}$ depict the input impedance of the magnetic tank from HV and LV side, respectively, and meanwhile, the inductor is connected only on low voltage side.

According to (1)~(4), the impedance of the magnetic tank can always be modeled as an LC parallel resonant circuit in series with the leakage inductance if there is only one inductor. Another LC parallel resonant circuit will be added to the model if there are two inductors. To make it clearer, the impedance model of the magnetic tank is also summarized in Table I.

It should be noted that the developed model is intended for high-frequency current ringing study. It guides converter hardware designers since it clearly shows how the different parasitic capacitance influence the current ringing with varying factors of weight. The developed model is not for the power flow control or output voltage control. The reason is that the parasitic capacitors have a minor impact on the power flow or

output voltage, which are therefore ignored in modeling for power flow control. However, the developed model is useful in gate voltage control or dv/dt control, which controls the slew rate of drain-source voltage during switching by controlling the gate voltage or gate resistance.

III. CURRENT RINGING ANALYSIS AND MITIGATION

A. Influence of the magnetic tank

As seen in Table I, if there is only one inductor in the magnetic tank, then to keep the equivalent inductance the same, it is required in the design of DAB that,

$$L_{ind,H} = n^2 L_{ind,L} \quad (9)$$

Therefore, the LV side input impedance $Z_{in,LV}$ always has an inductance n^2 times smaller than HV side input impedance $Z_{in,HV}$. That is why, in general, the current ringing is often observed in the LV side winding of the transformer rather than HV side. However, the impact of the parasitic capacitance is not considered so far. Secondly, for $Z_{in,HV}$, if the inductor is connected in HV side, the equivalent capacitance of the impedance is mainly the capacitance of the HV side inductor. If the inductor is connected in LV side, the equivalent capacitance of the impedance is dominated by the HV side winding capacitance and coupling capacitance of the transformer. Meanwhile, the impact of LV side winding capacitance and LV side inductor capacitance is attenuated by n^2 times. For $Z_{in,LV}$, if the inductor is connected in LV side, the equivalent capacitance of the impedance is mainly the capacitance of the

LV side inductor. If the inductor is connected in HV side, the equivalent capacitance of the impedance is affected mostly by the HV side inductor capacitance, the HV side winding capacitance and the coupling capacitance of the transformer.

B. Influence of dv/dt

Additionally, as discussed in Fig. 4, the current ringing is also influenced by the voltages v_{AB} and v_{CD} generated by both the HV and LV side full bridges. To be more specific, it is the dv/dt of v_{AB} and v_{CD} that affects the current ringing. For a thorough analysis, the spectrums of two trapezoidal waveforms are obtained, and they are shown in Fig. 7. Both of them have 50% duty ratio and the same magnitude, and only dv/dt differs. According to [62], the spectrums both have two corner frequencies. The first one is $f_s/0.5\pi$. Since it is lower than switching frequency f_s , it is invisible in the spectrum. The second corner frequency is $1/(\pi\tau)$, where τ is the rising time of the waveform. The two trapezoidal waveforms both have magnitude as ± 110 V. Thus the second corner frequency can be calculated with given dv/dt and they are $f_1 = 1.45$ MHz and $f_2 = 2.89$ MHz. Below the second corner frequency, the envelope of the spectrum decreases at a rate of -20 dB per decade, while above the second corner frequency, the envelope decreases at a rate of -40 dB per decade. Thus, it can be concluded that different dv/dt will lead to different second corner frequency and different magnitude of the spectrum after the second corner frequency. Higher the dv/dt , higher the magnitude of the spectrum after second corner frequency, higher the chance of current ringing.

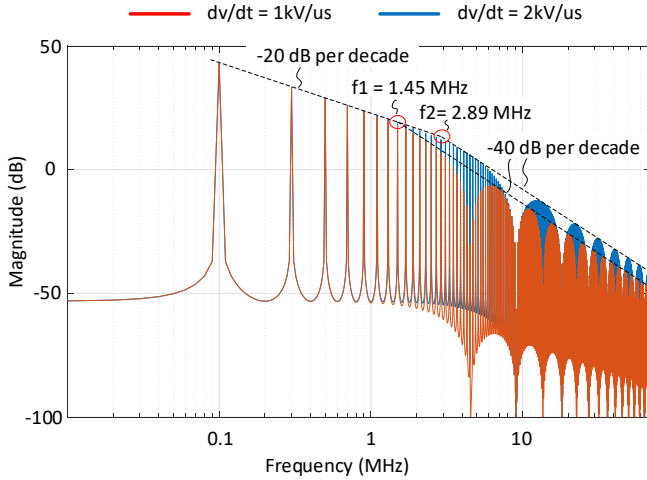
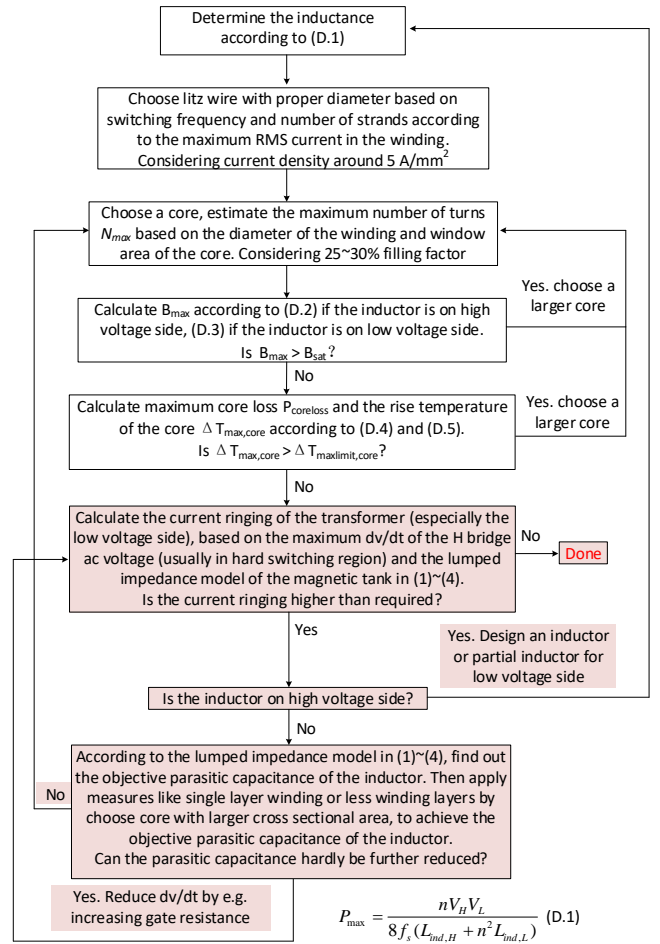


Fig. 7. Spectrum of trapezoidal waveforms @ $f_s = 100$ kHz with same magnitude but different dv/dt .

C. Current ringing mitigation

To mitigate the current ringing, one way is to increase the impedance of the magnetic tank at the frequency of interest; another is to slow down dv/dt . There are two typical approaches to slow down dv/dt :

- using larger gate resistance,
- adding more capacitance in parallel with the switches.



$$P_{\max} = \frac{nV_H V_L}{8f_s (L_{\text{ind},H} + n^2 L_{\text{ind},L})} \quad (\text{D.1})$$

$$B_{\max} = \frac{V_H + nV_L}{2N_{\max} f_s} \quad (\text{D.2})$$

$$B_{\max} = \frac{V_H / n + V_L}{2N_{\max} f_s} \quad (\text{D.3})$$

$$P_{\text{coreloss}} = kf_s V_{\text{core}} \Delta B^2 \quad (\text{D.4})$$

$$\Delta T_{\text{max,core}} = P_{\text{coreloss}} R_{\text{th,core}} \quad (\text{D.5})$$

Fig. 8. Flow chart of the inductor design procedure (the concern regarding current ringing is marked in color)

Both of the two approaches will increase the switching loss in case the converter operates in hard switching. As known, DAB will inevitably enter into hard switching mode when the load is very low, or the voltage deviates much from the optimal point. Even in soft-switching mode, although the switching loss will not increase, the switching frequency will be limited due to duty ratio loss. Therefore, for medium and high-frequency DAB, improving the magnetic tank is the better way to go for the transformer current ringing mitigation. And as analyzed above and commented in Table I, the most promising way is to add the inductor in the LV side of the transformer. Then the inductor capacitance is the only parameter needed to be minimized. All the other parasitic capacitances will have marginal influence. Experiments in Section V will verify this.

To summarize and give clear indication of design concerns regarding current ringing, a flow chart of the inductor design procedure is shown in Fig. 8. Since several steps are from the conventional inductor design procedure, only the design steps regarding current ringing are marked in color.

IV. EXPERIMENTAL VERIFICATION

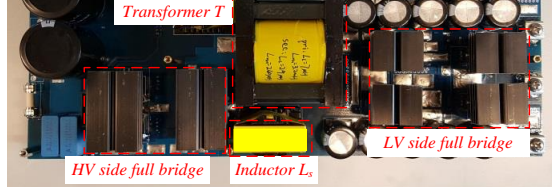


Fig. 9. A 2.5 kW dual active bridge converter prototype.

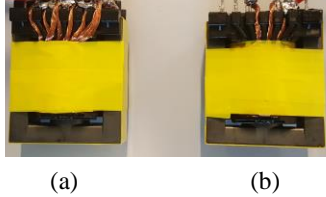


Fig. 10. The picture of the (a) LV (b) HV side inductor.

TABLE II. DESIGN PARAMETERS OF THE TRANSFORMER.

Parameter	Value
Core type	ETD 59
Core material	Ferrite N97
Primary winding	Litz wire \varnothing 0.2 mm, 90 strands in parallel, 21 turns
Secondary winding	Copper foil 0.15 mm x 35 mm, 2 layers in parallel, 6 turns

TABLE III. DESIGN PARAMETERS OF THE INDUCTORS.

Parameter	Value	
	Inductor L_H	Inductor L_L
Core type	ER42V (gapped)	
Core material	Ferrite N87	
Winding	Litz wire \varnothing 0.2 mm	
	90 strands in parallel, 17 turns	270 strands in parallel, 5 turns

TABLE IV. MEASURED PARAMETERS OF THE TRANSFORMER AND INDUCTORS

Parameter	Value	Parameter	Value
C_H	77 pF	$L_{ind,H}$	37.5 μ H
C_L	253 pF	$C_{ind,H}$	5.5 pF
C_{HL}	106 pF	$L_{ind,L}$	3.5 μ H
L_{leak}	8 μ H	$C_{ind,L}$	22 pF
L_m	2.5 mH	$R_{ind,H,fe}$	6.5 k Ω
R_{Tfe}	8.5 k Ω	$R_{ind,L,fe}$	800 Ω
R_{Tcu}	0.023 Ω	$R_{ind,H,cu}$	0.009 Ω
		$R_{ind,L,cu}$	0.0009 Ω

A 2.5 kW DAB prototype has been built for validation, as shown in Fig. 9. The switching frequency is 100 kHz, the nominal HV and LV side dc voltages are 400 V and 110 V, respectively. The switches used for HV and LV side are IPW65R080CFD and IPP110N20N3 (two in parallel), respectively.

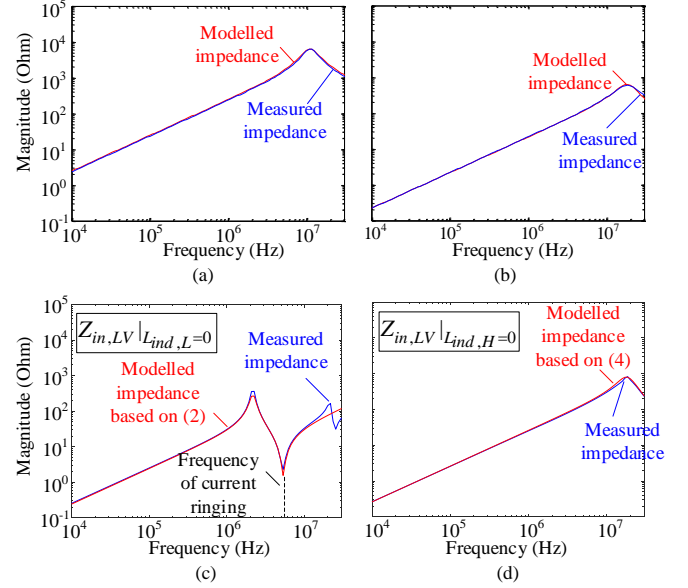


Fig. 11. Comparison between modeled and measured impedance of (a) HV side inductor (b) LV side inductor; LV side input impedance of the magnetic tank with (c) only HV side inductor (d) only LV side inductor.

The turns ratio of the transformer is $n = 3.5$. The design parameters of the transformer are listed in Table II. By using a KEYSIGHT E4990A Impedance Analyzer and the measurement approach in [10], the parameters of the transformer impedance model are obtained, and they are listed in Table IV. The design parameters of the inductors L_{HV} and L_{LV} are listed in Table III. To make a fair comparison between the two inductors, the same type of cores are used, as shown in Fig. 10, and both of their windings are designed as a single layer to minimize the parasitic capacitance [7]. The impedances of the two inductors are measured and shown in Fig. 11 (a) and (b). By fitting the curves based on the inductor impedance model in Fig. 3, the model parameters are obtained, and they are listed in Table IV. As seen in Fig. 11 (a) and (b), the inductor impedance model can match the measured impedance very well. Moreover, compared with the transformer, the winding capacitances of the inductors are much smaller even their number of turns are similar, which proves that the single layer winding structure is effective to reduce the parasitic capacitance. Since the current ringing more often occurs in the LV side winding of the transformer, only the LV side input impedance $Z_{in,LV}$ of the magnetic tank is tested, as shown in Fig. 11 (c) and (d). The fitting curves based on the simplified models of $Z_{in,LV}|_{L_{ind,L}=0}$ and $Z_{in,LV}|_{L_{ind,H}=0}$ in (2) and (4) are also shown. As seen, the simplified models can match the measured impedances very well. $Z_{in,LV}|_{L_{ind,L}=0}$ and $Z_{in,LV}|_{L_{ind,H}=0}$ are then compared in Fig. 12. As seen, they have the same value at low frequency, but $Z_{in,LV}|_{L_{ind,L}=0}$ has the first resonant frequency at 2 MHz. Above that, $Z_{in,LV}|_{L_{ind,L}=0}$ becomes capacitive and achieves the valley at 5 MHz. Meanwhile, $Z_{in,LV}|_{L_{ind,H}=0}$ has the first resonant frequency at 20 MHz, and the frequency of valley is, of course, higher than that, which reduces the chance of current

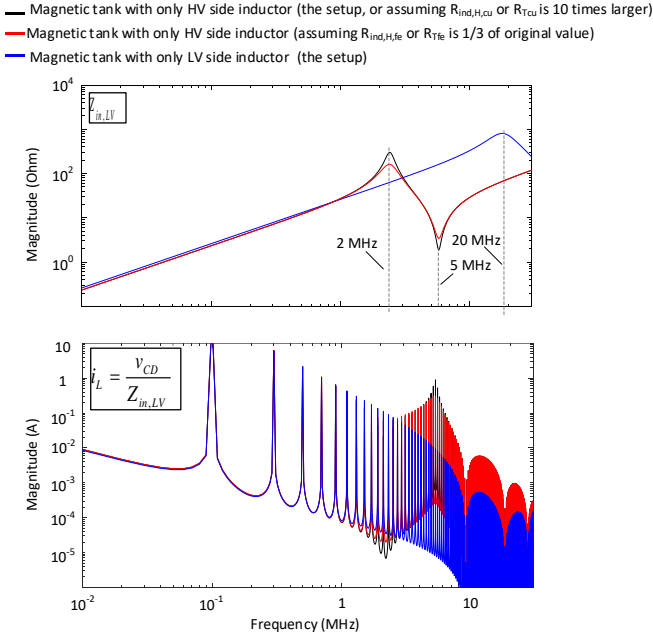


Fig. 12. The impedance of the magnetic tank and LV side current, influenced by the inductor and the resistance of the magnetic tank.

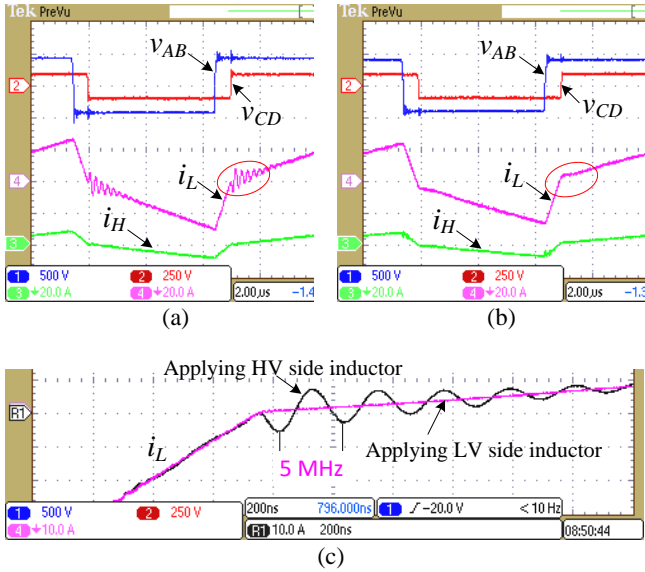


Fig. 13. Experimental results to show the transformer currents with (a) HV side inductor (b) LV side inductor (c) a zoom in

ringing a lot. The spectrum of $i_L = \frac{v_{CD}}{Z_{in,LV}}$ is then calculated, and it is shown in Fig. 12 as well, where dv/dt of v_{CD} is assumed to be 2 kV/us. As seen, a peak appears in the spectrum of the i_L with $Z_{in,LV}|_{L_{ind,L}=0}$ at 5 MHz, while it is not the case in the spectrum of the i_L with $Z_{in,LV}|_{L_{ind,H}=0}$. The test results in Fig. 13 (c) show that the current ringing happens in i_L at around 5 MHz if the HV side inductor is used. And there is no current ringing in i_L if the LV side inductor is used. Moreover, as seen in Fig. 13 (a) and (b), i_H has no or much smaller ringing, no

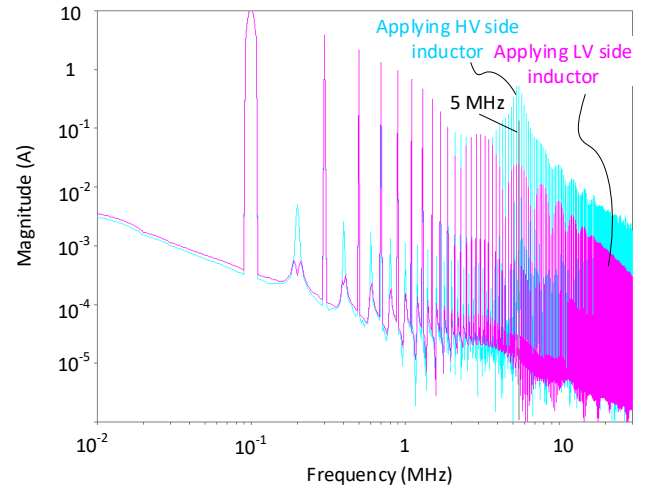


Fig. 14. FFT of i_L obtained in the experimental results.

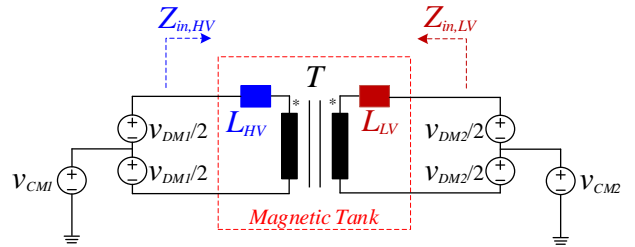


Fig. 15. Equivalent circuit of the DAB converter with the magnetic tank. v_{CM1} , v_{CM2} are the common-mode voltage sources, v_{DM1} , v_{DM2} are the differential mode voltage sources, respectively.

matter the HV or LV side inductor is used. The FFT of the i_L in Fig. 13(c) is also obtained, and it is shown in Fig. 14. As seen, it matches very well with the calculated FFT in Fig. 12. Besides, the impact of the resistance on impedance and current ringing is also indicated in Fig. 12. As seen, the core loss related to equivalent resistance can significantly influence the peak and valley of the impedance resonance, as well as the current ringing. And lower the resistance, lower the current ringing. However, in a proper design, the core loss should be minimized, which means the core loss related resistance cannot be too small. So it is impractical to mitigate the current ringing by reducing the core loss pertaining resistance. The copper loss related resistance does not have visible influence on the impedance curves, even they are 10 times larger.

The EMI equivalent circuit of the dual active bridge is derived in [54], and it is combined with the magnetic tank as in Fig. 15. As indicated in Fig. 12, compared with applying HV side inductor, applying the LV side inductor keeps a higher impedance in the DM noises loop from 5 to 30 MHz. Therefore, the DM current in the loop is decreased, as verified in Fig. 12, and Fig. 13. For the CM noise, the capacitance of the HV side inductor is with higher capacitance (5.5 pF) than the LV side inductor when it is transferred to the HV side (1.8 pF). This is due to the contribution of the larger core-related capacitance and the larger strands of Litz wire, which induces larger capacitance. In reality, the HF side inductor will have even larger capacitance due to its high number of turns. So, the multi-

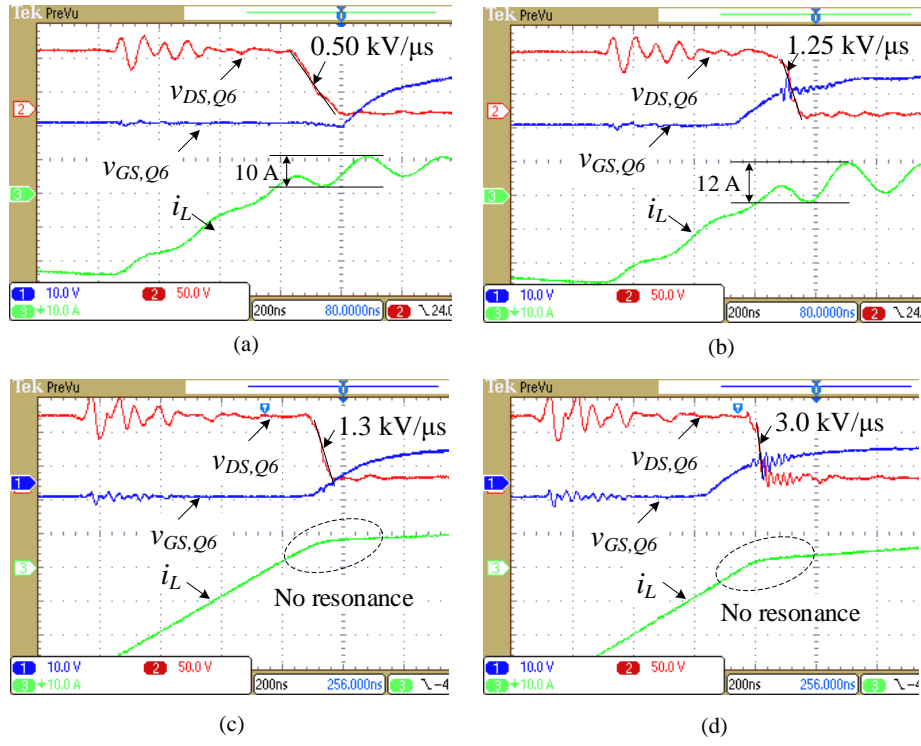


Fig. 16. Experimental results to show the impact of dv/dt and inductor on current ringing, where (a) and (b) has only HV side inductor, (c) and (d) has only LV side inductor.

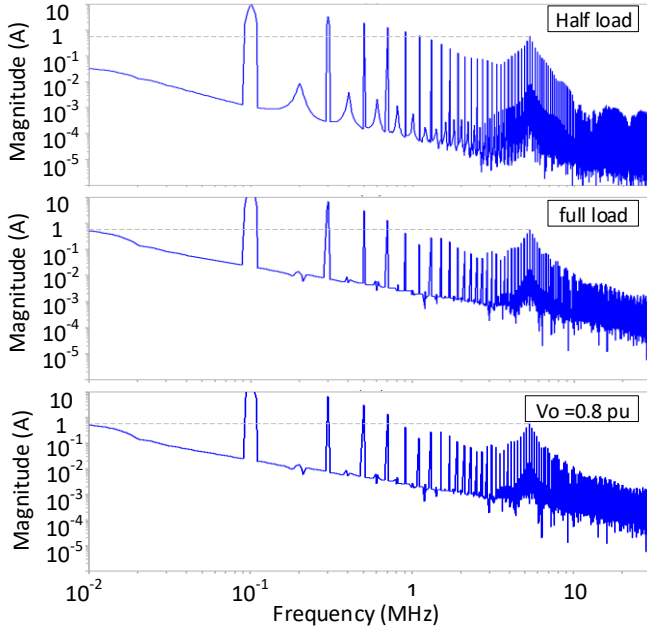


Fig. 17. FFT of i_L when HV side inductor is applied ($V_o=1$ pu if not specified)

layer-winding configuration is usually applied, resulting in significant winding capacitance. Therefore, there is also a smaller CM noise when only using the LV side inductor.

The impact of dv/dt on the current ringing is also tested, and it is shown in Fig. 16. As seen in Fig. 16 (a) and (b), when the the efficiency difference caused by the inductor design is quite marginal. The loss break down is analyzed to show a more concrete comparison in Fig. 19. In the top figure, the loss of

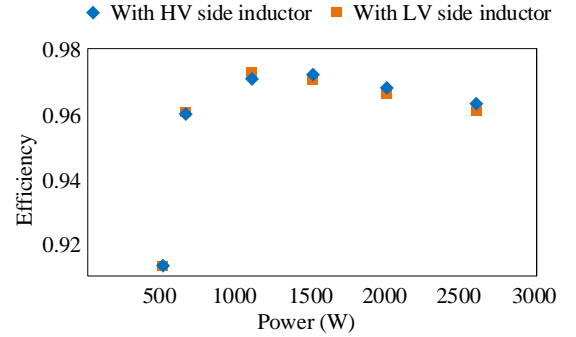


Fig. 18. The overall efficiency of the converter with two different inductor design.

most of the components remains the same between the two design. The transformer copper loss is supposed to be higher when HV side inductor is applied. It is due to the current ringing when using HV side inductor. The current ringing has very high frequency, and due to skin effect, the equivalent ac resistance of the transformer winding is also higher, leading to higher copper loss. The current ringing is mitigated when applying LV side inductor; therefore, the copper loss of the transformer is supposed to be lower. Nonetheless, the current ringing is small, and thereby the loss caused by the current ringing is marginal and has minimal impact on the efficiency. However, if C_H is five times larger, the loss of the transformer and inductor will be significantly influenced, as shown in the bottom figure.

V. CONCLUSIONS

In this paper, the current ringing issues in the DAB converter are thoroughly investigated. The impedance model of the magnetic tank is developed. It shows that the parasitic

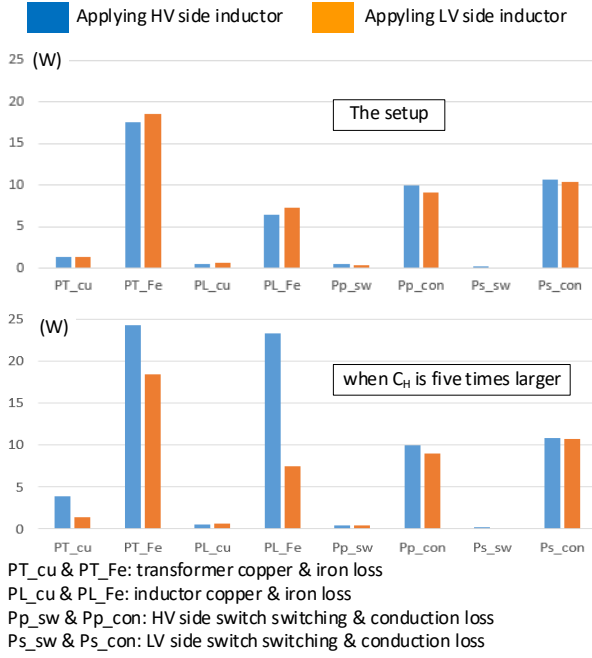


Fig. 19. Loss break down of the converter.

capacitors in the magnetic tank affect the current ringing with different weight factors. The position of the inductor and their parasitic capacitors can have a more significant influence on the current ringing than the transformer design. Additionally, the influence of dv/dt is analyzed, which is another factor that can significantly affect the current ringing. In the end, the conventional inductor design procedure is updated with the concern on current ringing.

APPENDIX

A. Modeling of $Z_{in,HV}$

According to Thevenin's Theorem, the effect of the LV side voltage v_{CD} can be eliminated by shorting it. Then by applying the transformer and inductor model in Fig. 2 and Fig. 3 into the magnetic tank, an equivalent circuit is obtained, and it is shown in Fig. 5 (a). For simplification, the secondary side components are all equivalent to the primary side, and the coupling capacitance C_{HL} is split into two, then the circuit in Fig. 5 (b) is obtained. L_{leak} is usually much smaller than $L_{ind,H}$, $L_{ind,L}$ and L_m . Moreover $L_m \gg L_{ind,H}$, thus the circuit is further simplified, as shown in Fig. 5 (c). According to the definitions of $v_{H,1}$, $v_{L,1}$ and $i_{L,1}$ in Fig. 5 (c), they follow,

$$\frac{C_{HL}}{2} d\left(\frac{v_{H,1}-v_{L,1}}{2}\right) = -i_{L,1} \quad (A.1)$$

According to Kirchhoff's Current Law (KCL), it is obtained,

$$i_1 = i_{H,1} - i_{L,1} \quad (A.2)$$

The voltages and currents of the transformer follow,

$$v_{L,1} = v_{H,1}/n \quad (A.3)$$

$$i_{L,1} = ni_{H,1} \quad (A.4)$$

Substitutes (A.2)~(A.4) into (A.1), it is obtained,

$$\frac{(1-1/n)^2 C_{HL}}{4} \frac{dv_{H,1}}{dt} = i_1 \quad (A.5)$$

According to (A.5), the transformer in Fig. 5(c) together with its coupling capacitance can be equivalent into a capacitor $(1-1/n)^2 C_{HL}/4$. Fig. 5(c) is then converted into Fig. 5 (d), which is the model of $Z_{in,HV}$.

B. Modeling of $Z_{in,LV}$

Similarly, to model $Z_{in,LV}$, an equivalent circuit of the magnetic tank is obtained, and it is shown in Fig. 6 (a). The HV side components will be equal to LV side, and the coupling capacitance is split into two. Then Fig. 6 (b) is obtained. L_{leak}/n^2 is much smaller than $L_{ind,L}$, $L_{ind,H}/n^2$ and L_m/n^2 . Moreover $L_m \gg n^2 L_{ind,L}$, thus Fig. 6 (b) is transformed to Fig. 6 (c). According to the definitions of $v_{H,2}$, $v_{L,2}$ and $i_{L,2}$ in Fig. 6 (c), they follow,

$$\frac{C_{HL}}{2} d\left(\frac{v_{H,2}-v_{L,2}}{2}\right) = -i_{H,2} \quad (A.6)$$

According to Kirchhoff's Current Law (KCL), it is obtained,

$$i_2 = i_{L,2} - i_{H,2} \quad (A.7)$$

The voltages and currents of the transformer follow,

$$v_{L,2} = v_{H,2}/n \quad (A.8)$$

$$i_{L,2} = ni_{H,2} \quad (A.9)$$

Substitutes (A.10)~(A.12) into (A.9), it is obtained,

$$\frac{(n-1)^2 C_{HL}}{4} \frac{dv_{L,2}}{dt} = -i_2 \quad (A.10)$$

According to (A.13), the transformer in Fig. 6 (c) together with its coupling capacitance can be equivalent into a capacitor $(n-1)^2 C_{HL}/4$. Fig. 6 (c) is then converted into Fig. 6 (d), which is the model of $Z_{in,LV}$.

REFERENCES

- [1] R. W. De Doncker, D. M. Divan, and et. al, "A Three-Phase Soft-Switched High Power Density DC/DC Converter for High Power Applications," in Proc. of IEEE Industry Applications Society Annual Meeting, vol. 1, Oct. 1988, pp. 796-805.
- [2] M. Liserre, G. Buticchi, M. Andresen, G. De Carne, L. F. Costa, Z.X. Zou, "The smart transformer: Impact on the electric grid and technology challenges," IEEE Industrial Electronics Magazine, vol. 10, no. 2, pp.46-58, 2016.
- [3] J. Ge, Z. Zhao, L. Yuan, T. Lu, "Energy Feed-Forward and Direct Feed-Forward Control for Solid-State Transformer," IEEE Trans. Power Electron. Vol. 30, no. 8, pp. 4042-4047, 2015.
- [4] B. Zhao, Q. Song, W. Liu, Y. Sun, "Overview of Dual-Active-Bridge Isolated Bidirectional DC-DC Converter for High-Frequency-Link Power-Conversion System," IEEE Trans. Power Electron., vol. 29, no. 8, pp. 4091-4106, 2014.
- [5] L. Xue, Z. Shen, D. Boroyevich, and et. al, "Dual Active Bridge-Based Battery Charger for Plug-in Hybrid Electric Vehicle With Charging Current Containing Low Frequency Ripple," IEEE Trans. Power Electron., vol. 30, no. 12, pp. 7299-7307, 2015.
- [6] S. Anwar, W. Zhang, F. Wang, and et. al, "Integrated dc-dc converter design for electric vehicle powertrains," in Proc. of APEC 2016, pp. 424-431, 2016.
- [7] S. P. Engel, M. Stieneker, N. Soltan, S. Rabiee, H. Stagge, R. W. De Doncker, "Comparison of the modular multilevel dc converter and the

- dual-active bridge converter for power conversion in HVDC and MVDC grids," *IEEE Trans. Power Electron.*, vol. 30, no. 1, pp. 124–137, 2015.
- [8] P. Purgat, R. A. Prakoso, L. Mackay, Z. Qin, L. Ramirez-Elizondo, P. Bauer, "A partially rated DC-DC converter for power flow control in meshed LVDC distribution grids," in *Proc. of APEC* 2018, pp. 1591–1596, 2018.
 - [9] P. Purgat, N. van der Blij, Z. Qin, P. Bauer, "Partially Rated Power Flow Control Converter Modeling for Low Voltage DC Grids," *IEEE Journal of Emerging and Selected Topics in Power Electronics* (Early Access), DOI: 10.1109/JESTPE.2019.2915166, 2019.
 - [10] J. Everts, F. Krismer, J. Van den Keybus, J. Driesen, J. W. Kolar, "Optimal ZVS Modulation of Single-Phase Single-Stage Bidirectional DAB AC-DC Converters," *IEEE Trans. Power Electron.*, vol. 29, no. 8, pp. 3954–3970, 2014.
 - [11] T. Todorčević, R. van Kessel, P. Bauer, J. A. Ferreira, "A modulation strategy for wide voltage output in DAB-based DC-DC modular multilevel converter for DEAP wave energy conversion," vol. 3, no. 4, pp. 1171–1181, 2015.
 - [12] Z. Qin, Y. Shen, P. C. Loh, H. Wang, F. Blaabjerg, "A dual active bridge converter with an extended high-efficiency range by DC blocking capacitor voltage control," *IEEE Trans. Power Electron.* Vol. 33, no. 7, pp. 5949–5966, 2018.
 - [13] B. Cui, P. Xue, X. Jiang, "Elimination of High Frequency Oscillation in Dual Active Bridge Converters by dv/dt Optimization," *IEEE Access*, vol. 7, pp. 55554–55564, 2019.
 - [14] R. T. Naayagi, "Electromagnetic compatibility issues of dual active bridge DC-DC converter," in *Proc. of ICEETS* 2013, pp. 699–703, 2013.
 - [15] Z. Shen, H. Wang, Y. Shen, Z. Qin and F. Blaabjerg, "An Improved Stray Capacitance Model for Inductors," in *IEEE Transactions on Power Electronics*. vol. 34, no. 11, pp. 11153–11170, 2019.
 - [16] J. Biela, and J. W. Kolar, "Using transformer parasitics for resonant converters—A review of the calculation of the stray capacitance of transformers," *IEEE Trans. Ind. Appl.*, vol. 44, no. 1, pp. 223–233, Jan./Feb. 2008.
 - [17] P. Thummala, H. Schneider, Z. Zhang, and M. A. E. Andersen, "Investigation of transformer winding architectures for high-voltage (2.5 kV) capacitor charging and discharging applications," *IEEE Trans. Power Electron.*, vol. 31, no. 8, pp. 5786–5796, Aug. 2016.
 - [18] B. Liu, R. Ren, F. Wang, D. Costinett, and Z. Zhang, "Winding scheme with fractional layer for differential-mode toroidal inductor," *IEEE Trans. Ind. Electron.*, vol. 67, no. 2, pp. 1592–1604, Feb. 2020.
 - [19] X. Liu, Y. Wang, J. Zhu, Y. Guo, G. Lei, and C. Liu, "Calculation of capacitance in high-frequency transformer windings," *IEEE Trans. Magn.*, vol. 52, no. 7, pp. 1–4, Jul. 2016.
 - [20] M. S. S. Nia, P. Shamsi, and M. Ferdowsi, "Investigation of various transformer topologies for HF isolation applications," *IEEE Trans. Plasma Sci.*, pp. 1–10, 2020.
 - [21] R. Chattopadhyay, M. A. Judo, P. R. Ohodnicki and S. Bhattacharya, "Modelling, design and analysis of three limb high frequency transformer including transformer parasitics, for SiC Mosfet based three port DAB," *IEEE IECON* 2016, 2016, pp. 4181–4186.
 - [22] L. F. de Freitas Gutierrez and G. C. Junior, "Analytical technique for evaluating stray capacitances in multiconductor systems: Single layer air-core inductors," *IEEE Trans. Power Electron.*, vol. 33, no. 7, pp. 6147–6158, Jul. 2018.
 - [23] M. Aghaei and S. Kaboli, "On the effect of disorder on stray capacitance of transformer winding in high-voltage power supplies," *IEEE Trans. Ind. Electron.*, vol. 64, no. 5, pp. 3608–3618, May 2017.
 - [24] Z. Shen and H. Wang, "Parasitics of Orthocyclic Windings in Inductors and Transformers," *IEEE Trans. Power Electron.*, Early access.
 - [25] Z. Ouyang, O. C. Thomsen, and M. A. E. Andersen, "Optimal design and tradeoff analysis of planar transformer in high power dc-dc converters," *IEEE Trans. Ind. Electron.*, vol. 59, no. 7, pp. 2800–2810, July 2012.
 - [26] M. A. Saket, N. Shafiei, and M. Ordonez, "LLC converters with planar transformers: Issues and mitigation," *IEEE Trans. Power Electron.*, vol. 32, no. 6, pp. 4524–4542, Jun. 2017.
 - [27] L. A. R. Tria, D. Zhang, and J. E. Fletcher, "High-frequency planar transformer parameter estimation," *IEEE Trans. Magn.*, vol. 51, no. 11, pp. 1–4, Nov. 2015.
 - [28] P. L. Dowell, "Effects of eddy currents in transformer windings," *Proc. Inst. Electr. Eng.*, vol. 113, no. 8, pp. 1387–1394, Aug. 1966.
 - [29] D. Whitman and M. K. Kazimierczuk, "An analytical correction to Dowell's equation for inductor and transformer winding losses using cylindrical coordinates," *IEEE Trans. Power Electron.*, vol. 34, no. 11, pp. 10 425–10 432, Nov. 2019.
 - [30] M. Bahmani, T. Thiringer, and H. Ortega, "An accurate pseudoempirical model of winding loss calculation in HF foil and round conductors in switchmode magnetics," *IEEE Trans. Power Electron.*, vol. 29, no. 8, pp. 4231–4246, Aug. 2014.
 - [31] C. Feeney, J. Zhang, and M. Duffy, "Ac winding loss of phase shifted coupled windings," *IEEE Trans. Power Electron.*, vol. 31, no. 2, pp. 1472–1478, 2015.
 - [32] B. A. Reese and C. R. Sullivan, "Litz wire in the MHz range: Modeling and improved designs," in *Proc. 2017 IEEE COMPEL*, 2017, pp. 1–8.
 - [33] E. Barrios, A. Ursua, L. Marroyo, and P. Sanchis, "Analytical design methodology for litz-wired high-frequency power transformers," *IEEE Trans. Ind. Electron.*, vol. 62, no. 4, pp. 2103–2113, Apr. 2015.
 - [34] R. P. Wojda and M. K. Kazimierczuk, "Winding resistance and power loss of inductors with litz and solid-round wires," *IEEE Trans. Ind. Appl.*, vol. 54, no. 4, pp. 3548–3557, 2018.
 - [35] Z. Ouyang, J. Zhang, and W. G. Hurley, "Calculation of leakage inductance for high-frequency transformers," *IEEE Trans. Power Electron.*, vol. 30, no. 10, pp. 5769–5775, Oct. 2015.
 - [36] M. A. Bahmani and T. Thiringer, "Accurate evaluation of leakage inductance in high-frequency transformers using an improved frequency dependent expression," *IEEE Trans. Power Electron.*, vol. 30, no. 10, pp. 5738–5745, Oct. 2015.
 - [37] A. Fouineau, M. Raulet, B. Lefebvre, N. Burais, and F. Sixdenier, "Semi-analytical methods for calculation of leakage inductance and frequency-dependent resistance of windings in transformers," *IEEE Trans. Magn.*, vol. 54, no. 10, pp. 1–10, Oct. 2018.
 - [38] K. Zhang, W. Chen, X. Cao, P. Pan, S. W. Azeem, G. Qiao, and F. Deng, "Accurate calculation and sensitivity analysis of leakage inductance of high-frequency transformer with litz wire winding," *IEEE Trans. Power Electron.*, vol. 35, no. 4, pp. 3951–3962, Apr. 2020.
 - [39] F. Pan, L. Jin, P. Pan, and Z. Xu, "Design procedure of the leakage inductance for a pulse transformer considering winding structures," *IEEE Trans. Plasma Sci.*, vol. 45, no. 9, pp. 2504–2510, Sep. 2017.
 - [40] M. Nazmunnahar, S. Simizu, P. R. Ohodnicki, S. Bhattacharya, and M. E. McHenry, "Finite-element analysis modeling of high-frequency single-phase transformers enabled by metal amorphous nanocomposites and calculation of leakage inductance for different winding topologies," *IEEE Trans. Magn.*, vol. 55, no. 7, pp. 1–11, Jul. 2019.
 - [41] R. Chattopadhyay, M. A. Judo, G. Gohil, S. Guler, P. R. Ohodnicki and S. Bhattacharya, "Optimized design for three port transformer considering leakage inductance and parasitic capacitance," *IEEE ECCE*, 2017, pp. 3247–3254.
 - [42] Z. Ouyang, W. G. Hurley, and M. A. E. Andersen, "Improved analysis and modeling of leakage inductance for planar transformers," *IEEE Trans. Emerg. Sel. Topics Power Electron.*, vol. 7, no. 4, pp. 2225–2231, Dec. 2019.
 - [43] M. Zdanowski, J. Rabkowski, K. Kostov, J. Rabkowski, R. Barlik, H.P. Nee, "Design and Evaluation of Reduced Self-Capacitance Inductor in DC/DC Converters with Fast-Switching SiC Transistors," *IEEE Trans. Power Electron.*, vol. 29, no. 5, pp. 2492–2499, 2014.
 - [44] J. C. Hernandez, L. P. Petersen, M. A. E. Andersen, "Low Capacitive Inductors for Fast Switching Devices in Active Power Factor Correction Applications," in *Proc. of IPEC* 2014, pp. 3352–3357, 2014.
 - [45] M. Pahlevaninezhad, D. Hamza and P. K. Jain, "An Improved Layout Strategy for Common-Mode EMI Suppression Applicable to High-Frequency Planar Transformers in High-Power DC/DC Converters Used for Electric Vehicles," *IEEE Trans. Power Electron.*, vol. 29, no. 3, pp. 1211–1228, March 2014.
 - [46] M. A. Saket, M. Ordonez, and N. Shafiei, "Planar transformers with near-zero common-mode noise for flyback and forward converters," *IEEE Trans. Power Electron.*, vol. 33, no. 2, pp. 1554–1571, Feb. 2018.
 - [47] Y. Li, H. Zhang, S. Wang, H. Sheng, C. P. Chng, and S. Lakshmikanthan, "Investigating switching transformers for common mode EMI reduction to remove common mode EMI filters and y-capacitors in flyback converters," *IEEE Trans. Emerg. Sel. Topics Power Electron.*, vol. 6, no. 4, pp. 2287–2301, Dec. 2018.
 - [48] Z. Shen et al., "The Faraday Shields Loss of Transformers," *IEEE Trans. Power Electron.*, vol. 35, no. 11, pp. 12194–12206, Nov. 2020.
 - [49] Z. Yang, J. Hu, G. C. Pasupuleti and R. W. De Doncker, "Operation-Oriented Design Procedure of a Three-Phase Dual-Active Bridge

Converter for a Wide Operation Range," in Proc. IEEE ECCE, 2018, pp. 2835-2842.

- [50] M. Noah, T. Shirakawa, K. Umetani, J. Imaoka, M. Yamamoto, and E. Hiraki, "Effects of secondary leakage inductance on the LLC resonant converter," IEEE Trans. Power Electron., vol. 35, no. 1, pp. 835-852, Jan. 2020.
- [51] J. Riedel, D. G. Holmes, B. P. McGrath and C. Teixeira, "Active Suppression of Selected DC Bus Harmonics for Dual Active Bridge DC-DC Converters," IEEE Trans. Power Electron., vol. 32, no. 11, pp. 8857-8867, Nov. 2017.
- [52] Z. Qin, Z. Shen, F. Blaabjerg, P. Bauer, "Modelling, Analysis and Mitigation of the Transformer Current Ringing in Dual Active Bridge Converters," in Proc. of IEEE-ECCE' 2018, pp. 650-655, 2018
- [53] Module 3: Signals and Spectra. Online available: https://www.egr.msu.edu/emrg/sites/default/files/content/module3_signals_and_spectra.pdf
- [54] G. Buticchi, D. Barater, L. F. Costa and M. Liserre, "A PV-Inspired Low-Common-Mode Dual-Active-Bridge Converter for Aerospace Applications," IEEE Trans. Power Electron., vol. 33, no. 12, pp. 10467-10477, Dec. 2018.



Zian Qin (M'15-SM'19) received the B.Eng. degree in Automation from Beihang University, Beijing, China, in 2009, M.Eng. degree in Control Science and Engineering from Beijing Institute of Technology, Beijing, China, in 2012, and Ph.D. degree from Aalborg University, Aalborg, Denmark, in 2015.

He is currently an Assistant Professor in Delft University of Technology, Delft, Netherlands. In 2014, he was a Visiting Scientist at Aachen University, Aachen, Germany. From 2015 to 2017, he was a Postdoctoral Research Fellow in Aalborg University. His research interests include wide bandgap devices, power electronics based grid and Power2X. He serves as the technical program chair of IEEE-ISIE 2020, technical program co-chair of IEEE-COMPEL 2020, industrial session co-chair of ECCE-Asia 2020.



Zhan Shen (S'16-M'20) received the B.E. degree in electrical engineering and automation from Nanjing University of Aeronautics and Astronautics in 2013, and M.E. degree in electrical engineering from Southeast University in 2016, both in Nanjing, China, and the Ph.D. degree in power electronics from Center of Reliable Power Electronics, Aalborg University, Aalborg, Denmark, in 2020.

He is currently a Postdoctoral Research Fellow with Aalborg University. He was a Visiting Scholar with the Massachusetts Institute of Technology (MIT),

Cambridge, MA, USA, from Oct. 2018 to Jan. 2019, and a Visiting Student and pursued his master thesis at the RWTH Aachen University, Aachen, Germany, from Oct. 2014 to Feb. 2016. He was with the ABB Corporate Research Center, Beijing, China, in 2016. His research interests include modeling, design, and life-cycle performance optimization of magnetic components and EMI filters in power electronics.



Frede Blaabjerg (S'86-M'88-SM'97-F'03) was with ABB-Scandia, Randers, Denmark, from 1987 to 1988. From 1988 to 1992, he got the PhD degree in Electrical Engineering at Aalborg University in 1995. He became an Assistant Professor in 1992, an Associate Professor in 1996, and a Full Professor of power electronics and drives in 1998. From 2017 he became a Villum Investigator. He is honoris causa at University Politehnica Timisoara (UPT), Romania and Tallinn Technical University (TTU) in Estonia.

His current research interests include power electronics and its applications such as in wind turbines, PV systems, reliability, harmonics and adjustable speed drives. He has published more than 600 journal papers in the fields of power electronics and its applications. He is the co-author of four monographs and editor of ten books in power electronics and its applications.

He has received 32 IEEE Prize Paper Awards, the IEEE PELS Distinguished Service Award in 2009, the EPE-PEMC Council Award in 2010, the IEEE William E. Newell Power Electronics Award 2014, the Villum Kann Rasmussen Research Award 2014, the Global Energy Prize in 2019 and the 2020 IEEE Edison Medal. He was the Editor-in-Chief of the IEEE TRANSACTIONS ON POWER ELECTRONICS from 2006 to 2012. He has been Distinguished Lecturer for the IEEE Power Electronics Society from 2005 to 2007 and for the IEEE Industry Applications Society from 2010 to 2011 as well as 2017 to 2018. In 2019-2020 he serves a President of IEEE Power Electronics Society. He is Vice-President of the Danish Academy of Technical Sciences too.

He is nominated in 2014-2019 by Thomson Reuters to be between the most 250 cited researchers in Engineering in the world.



Pavol Bauer (SM'07) is currently a full Professor with the Department of Electrical Sustainable Energy of Delft University of Technology and head of DC Systems, Energy Conversion and Storage group. He received Masters in Electrical Engineering at the Technical University of Kosice (a85), Ph.D. from Delft University of Technology (a95) and title prof. from the president of Czech Republic at the Brno University of Technology (2008) and Delft University of Technology (2016). He published over 72 journal and almost 300 conference papers in my field (with H factor Google scholar 43, Web of science 20), he is an author or co-author of 8 books,

holds 4 international patents and organized several tutorials at the international conferences. He has worked on many projects for industry concerning wind and wave energy, power electronic applications for power systems such as Smarttrafo; HVDC systems, projects for smart cities such as PV charging of electric vehicles, PV and storage integration, contactless charging; and he participated in several Leonardo da Vinci and H2020 EU projects as project partner (ELINA, INETELE, E-Pragmatic) and coordinator (PEMCWebLab.com-Edipe, SustEner, Eranet DCMICRO).